

ESTIMATIVAS NUMÉRICAS DO TRABALHO PLÁSTICO ATÉ A INICIAÇÃO DA FRATURA POR RASGAMENTO*

Luiz Fernando Nazaré Marques¹

Eduardo Enes Cota²

Jaime Tupiassú Pinho de Castro²

Luiz Fernando Martha²

Marco Antonio Meggiolaro²

Resumo

Zonas plásticas (z_p) 3D em torno de frentes de trincas são estimadas por cálculos elastoplásticos (EP) de elementos finitos (EF) em componentes trincados com várias restrições transversais. Inicialmente, a técnica de submodelagem por EF é validada através de resultados da literatura. Além disso, para melhorar o cálculo de volume da z_p , a menor unidade de volume considerada é 1/8 do volume do elemento. Em seguida, são realizados experimentos para medir as curvas J-R utilizando corpos de prova SEB em aço API 5L X80, seguindo a norma ASTM E1820. Finalmente, os resultados numéricos são validados através de comparações diretas com resultados experimentais para valores de trabalho plástico e de deslocamentos medidos na superfície do corpo de prova, usando técnicas de correlação de imagem digital 3D. As comparações entre os resultados numéricos e experimentais indicam boas correlações.

Palavras-chave: Elementos finitos 3D; Mecânica da fratura elastoplástica (MFEP); Estimativas de zonas plásticas; Cálculos/Medições de trabalho plástico; Ensaio de resistência à fratura.

NUMERICAL PLASTIC WORK ESTIMATES UNTIL CRACK TEARING

Abstract

3D plastic zones (p_z) around crack fronts are estimated by elastoplastic (EP) finite element (FE) calculations for cracked components with different transversal constraints. First, the sub-modeling FE technique is validated through results taken from the literature. In addition, to improve the calculation of p_z volumes, the smallest unit of volume is chosen as 1/8 of the volume element. Experiments are performed to measure J-R curves using SEB specimens made of API 5L X80 steel, following ASTM E1820 standard procedures. Finally, the numerical results are validated through direct comparison with experimental results for the plastic work values, and for displacements measured on the surface of the specimen using 3D digital image correlation techniques. Comparisons between numerical and experimental results indicate good correlations.

Keywords: 3D finite elements; Elastoplastic Fracture Mechanics (EPFM); Plastic zone estimates; Plastic work calculations/measurements; Fracture resistance tests.

¹ *Federal University of South and Southeast of Pará (UNIFESSPA), Marabá - PA - Brazil.*

² *Pontifical Catholic University of Rio de Janeiro (PUC-Rio), Rio de Janeiro - RJ- Brazil.*

1 INTRODUCTION

Stress and strain fields around sharp crack fronts, which always have significant three-dimensional (3D) gradients, are the primary cause for crack propagation, stable tearing, and unstable fracture. Hence, the calculation of these fields is essential in engineering problems that involve fatigue and fracture assessments.

For designs and assessments based on fracture mechanics principles, the most important material parameter is the fracture toughness, or its ability to resist crack growth. Under Linear Elastic Fracture Mechanics (LEFM) conditions associated with brittle fractures, it can be quantified by K_{IC} , the critical Stress Intensity Factor (SIF) in mode I. For Elastic Plastic Fracture Mechanics (EPFM) conditions related with ductile fractures, it can be quantified by the energy per unit area J_{IC} needed to initiate the crack. These parameters allow engineers to select the material for their structures, or to evaluate cracks found in them. However, the actual fracture toughness of most practical structures depends not only the material, but can vary as well depending on their geometry and on the type of loading. Hence, the material toughness measured by standard procedures (1) tend to be conservative when compared with the actual toughness of most practical structures.

This article assumes that EP toughnesses can be estimated from the EP work spent to form the 3D plastic zones ahead of the crack fronts, which since Griffith is known to be much higher than the work needed to form two new surfaces during the crack growth process. Hence, using a properly validated model, elastoplastic (EP) finite element (FE) 3D calculations are performed to estimate sizes, shapes and EP works inside the plastic zones pz formed ahead of the crack front in highly-constrained and in lightly-constrained components (2). The 3D EP sub-modeling FE technique used in this work is validated through direct comparison with recently published numerical and experimental results for Middle Tension (MT) and CT specimens (3, 4).

To verify their predictions, J-R curves are measured using Single Edge Bending (SEB) specimens following ASTM E1820 testing procedures. To do so, the numerical results obtained using the 3D EP FE model are compared with the experimental results obtained for the plastic (PL) work up to the measured toughness values J_{IC} , and with displacements measured on the surface of the specimen using 3D Digital Image Correlation (DIC) techniques.

2 THREE-DIMENSIONAL PLASTIC ZONE ANALYSIS

The first purpose of this analysis is to show how the pz volume can vary significantly for a given K_I , directly contradicting a fundamental hypothesis usually assumed in traditional Fracture Mechanics estimates (5). Since both the material toughness and its resistance to fatigue crack growth depend on the EP work performed inside the pz , neglecting this fact this can have a major practical importance in many fracture and fatigue assessments. To support this statement, several EP FE 3D calculations are performed for constant K_I , varying the loading conditions represented by nominal stress/yield strength (σ_n/S_Y) ratios, and the geometry parameters represented by crack length/specimen width (a/W) and specimen width/specimen thickness (W/B).

For each simulated geometry, a 3D EP global FE model is generated and meshed using properly refined elements around the crack front, but increasing their size in regions away from it to limit the models size without compromising their accuracy. MT, CT, SET and SEB specimens are used in this study. From the solution of the global model, the EP frontiers of the pz in terms of the equivalent Mises strain are

mapped to ensure that the total volume of the pz is entirely within the sub-model with meshes of uniform element size for the final solution. The properties of the materials used in all simulations are presented in (Table 1), where E is Young's modulus, ν is Poisson's coefficient, S_Y is yielding strength, while H , h , H' , and h' are the monotonic and cyclic Ramberg-Osgood hardening coefficients and exponents.

Table 1. Materials and properties.

Material	E [GPa]	ν [1]	S_Y [MPa]	H [MPa]	h [1]	H' [MPa]	H/E [1]
2024-T3	73.1	0.33	345	-	-	984	-
2024-T351	73.5	0.33	425	685	0.073	220.5	0.003
API 5L X80	223	0.30	527	946	0.148	-	-

Both aluminum alloys are used to validate the model based on results taken from the literature (3, 4). The 2024-T3 Al is used to estimate pz sizes, shapes and EP works in highly-constrained CT and lightly-constrained SET specimens. The API 5L X80 steel is used to perform a direct comparison with experimental results obtained during this work. The EP work spent inside the pz until the measured J_{IC} is taken into account following ASTM E1820 testing procedures, and the displacements are measured on the surface of the specimens using 3D DIC techniques.

There are standard K_I -expressions for all specimens selected for this study, namely $K_I = [P/\sqrt{(B \cdot B_N \cdot W)}] \cdot f(a/W)_{\text{Specimen}}$, where B_N is the net thickness due to side grooves and $f(a/W)_{\text{Specimen}}$ is a geometry function that depends on the crack size to specimen width (a/W) ratio (1-6). Equations (1-4) present these functions for the MT, CT, SET, and SEB specimens. The SEB specimen geometry is shown in Figure 1.

$$f\left(\frac{a}{W}\right)_{MT} = \sqrt{\frac{2.25 \left(\frac{a}{W}\right)^2 \sec^2 \left(\frac{a}{W}\right)}{4W}} - 0.025 \left(\frac{a}{W}\right)^2 + 0.06 \left(\frac{a}{W}\right)^4 \quad (1)$$

$$f\left(\frac{a}{W}\right)_{CT} = \frac{2.25 \left(\frac{a}{W}\right)^2 + \frac{a}{W}}{2.25 \left(\frac{a}{W}\right)^2 - \frac{a}{W}} \cdot 8.86 + 4.64 \left(\frac{a}{W}\right) - 13.32 \left(\frac{a}{W}\right)^2 + 14.72 \left(\frac{a}{W}\right)^3 - 5.6 \left(\frac{a}{W}\right)^4 \quad (2)$$

$$f\left(\frac{a}{W}\right)_{SET} = \frac{\sqrt{2 \tan \left(\frac{a}{W}\right)}}{\cos \left(\frac{a}{W}\right)} \cdot 7.52 + 2.02 \left(\frac{a}{W}\right) + 0.37 \left(\frac{a}{W}\right)^3 - \sin \left(\frac{a}{W}\right) \quad (3)$$

$$f\left(\frac{a}{W}\right)_{SEB} = \frac{3 \left(\frac{a}{W}\right)^{1/2} \left[1.99 - \left(\frac{a}{W}\right) \left(1 - \frac{a}{W}\right) \left(2.15 - 3.93 \left(\frac{a}{W}\right) + 2.7 \left(\frac{a}{W}\right)^2 \right) \right]}{2 \left(1 + 2 \frac{a}{W}\right) \left(1 - \frac{a}{W}\right)^{3/2}} \quad (4)$$

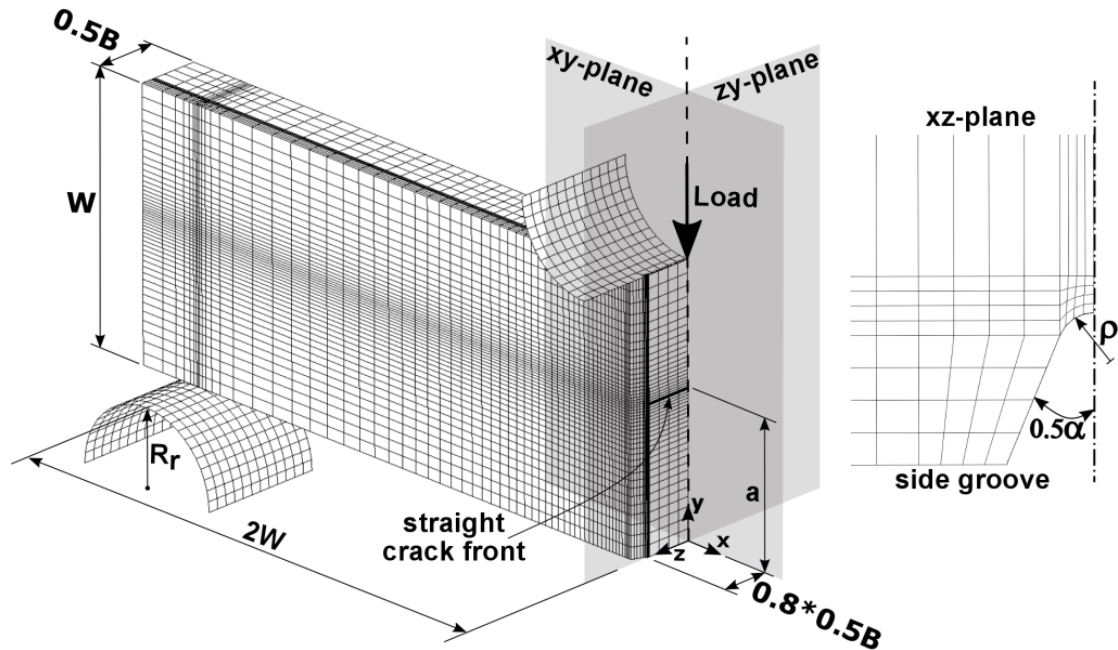


Figure 1. SEB specimen geometry and side groove detail.

2.1 FE validation

First, to validate the FE numerical analysis using the ANSYS software (7), a comparison is performed with two recent 3D results taken from the literature (3, 4) for the MT and CT specimens, respectively. In the global model, since a less refined mesh is required, it uses larger 3D SOLID186 elements with 20 nodes each and 8 Gauss integration points per element. A mesh convergence study is performed based on evaluations of the total volume (V_t) of the pz developed around the crack front for different mesh sizes. Figure 2 shows the shape and volume of only 1/4 of the pz on a MT specimen with 5 mm thickness for $K_I = 30 \text{ MPa}\sqrt{\text{m}}$. The same criterion is adopted here and a similar value for V_t (19.96 mm^3) is obtained (3). Figure 3 shows the numerical vertical displacements around the crack front on a CT specimen with ratios $a/W = 0.74$, $W/B = 7.25$ and 10 mm thickness for $K_I = 17.82 \text{ MPa}\sqrt{\text{m}}$ at three different vertical levels, and compares these results with those obtained from reference (4).

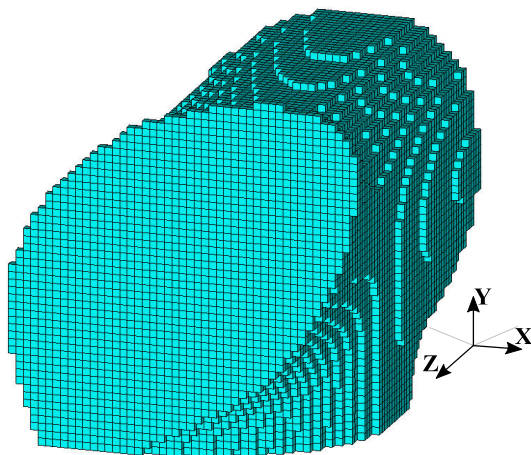


Figure 2. 1/4 shape and volume of the pz developed around the crack front on an MT specimen for $K_I = 30 \text{ MPa}\sqrt{\text{m}}$.

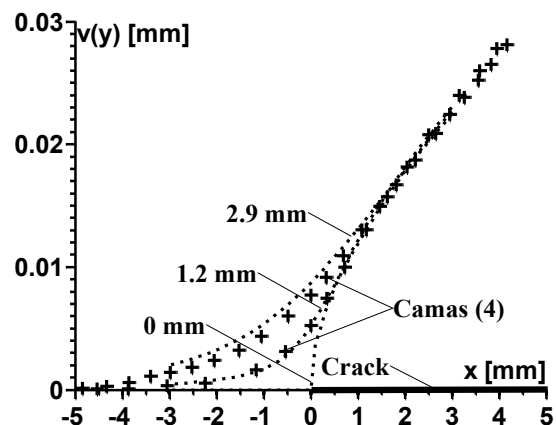


Figure 3. Numerical vertical displacement on CT specimen for $K_I = 17.82 \text{ MPa}\sqrt{\text{m}}$ on the crack plane and 1.20 mm and 2.90 mm from the crack plane.

2.2 FE verification

Despite the good agreement with the referenced results, the criterion for selection of the smallest unit considered in the pz can be improved. The smallest unit of volume considered in the pz is the volume of the full element (V_e) adopted in the modeling made by reference (3), which estimates the size of the pz based on the FEs that have Mises strain higher than yield strain ($\varepsilon_Y = S_Y/E$) in one of its integration points. The improvement of the calculation of pz volumes considers one eighth of the volume of the element ($V_e/8$) as the smallest unit of volume that corresponds to each Gauss integration point.

Before analyzing the sub-models used in this work, a mesh convergence study is performed to establish the mesh refinement parameters needed for the simulations. Such convergence tests are performed using the sub-modeling procedure described in the previous section. All 3D EP FE analyses are run on a desktop computer with 8 GB installed memory (RAM) and an Intel Core i7-9790 CPU clocking at 3.60 GHz. The verification is carried out through numerical simulations using both criteria (V_e and $V_e/8$) and the same FE model presented in Figure 2.

The 3D SOLID185 (linear) elements with 8 nodes each and the 3D SOLID186 (quadratic) elements with 20 nodes each are used, both with 8 integration points per element. Figure 4 shows the variation of the total pz volume (V_t) as a function of the number of elements along the modelled thickness $B/2$ for 3 different cases, where E_s is the element size. The first one is the adopted case for reference (3), which uses linear elements and V_e as the criterion to calculate the V_t of pz . The second case also uses linear elements but the $V_e/8$ criterion, while the third uses quadratic elements with the improved criterion.

For the first case, V_t of the pz converges to 9.9mm^3 after 35 elements along $B/2$. The second case achieves $V_t = 9.1\text{mm}^3$ after 30 elements. Finally, the last case achieves the same volume with only 15 elements. To evaluate the efficiency of the improved criterion used in this work, a comparison is performed between the latter two cases.

The computation CPU time required to evaluate the sub-model with 79,135 nodes and 69,120 linear elements is 19min12s; on the other hand, the sub-model with 38,575 nodes and 8,640 quadratic elements demands only 8min19s. Therefore, the sub-model with quadratic elements reaches the same result using 43% of the CPU time to solve the sub-model with linear elements. In addition, when the V_e criterion is taken into account, the V_t of the pz result in conservative predictions, as it can be seen in Figure 4. The same tendency is noted when the calculated EP work (U_{EP}) is evaluated in the convergence analysis (Figure 5). As a result, 15 elements along $B/2$ and the $V_e/8$ improved criterion to estimate the V_t of the pz are used for further analyses.

2.3 Numerical results for two differently constrained specimens

For CT and SET specimens with $K_I = 30 \text{ MPa}\sqrt{\text{m}}$, Figure 6 shows that the volume of the pz ahead of the crack front represented by the dimensionless ratio between the total volume of pz and the volume of the element (V_t/V_e) can vary significantly for a given SIF K_I . A quite remarkable difference in this V_t/V_e ratio can be seen through a comparison between two cases: an SET specimen with geometry and loading ratios $W/B = 4$, $a/W = 0.6$, and $\sigma_r/S_Y = 0.2$, and a CT specimen with $W/B = 4$, $a/W = 0.4$, and $\sigma_r/S_Y = 0.8$. A surprisingly huge factor of 24.2 is observed between them.

Overall, the same trend is noted when the EP work is evaluated (Figure 7). However, the factor decreases to 1.9, which is also a large difference. Hence, based on EP work arguments ahead of the crack front, it is possible to argue that measured toughness values J_{IC} may also dramatically change in those specimens.

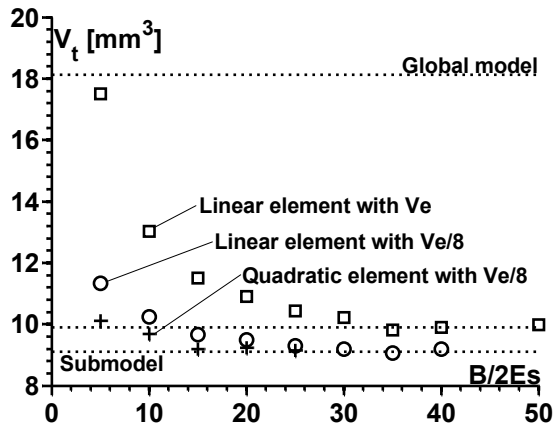


Figure 4. Analysis of the V_t of pz for three different cases.

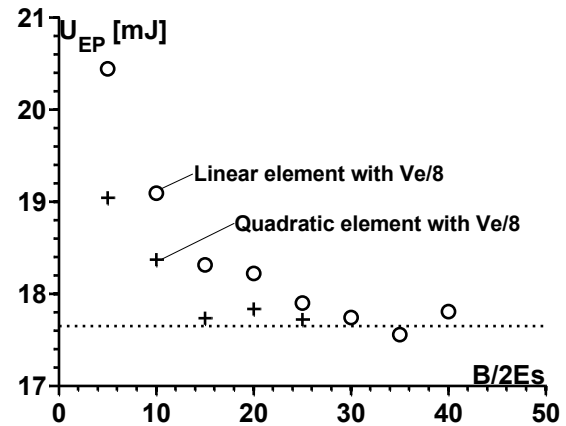


Figure 5. Analysis of the EP work (U_{EP}) inside the pz for cases with the $V_e/8$ improved criterion.

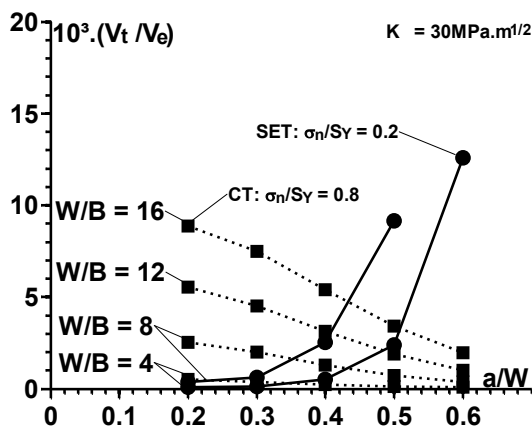


Figure 6. Total pz volumes ahead of the crack front for several simulated cases.

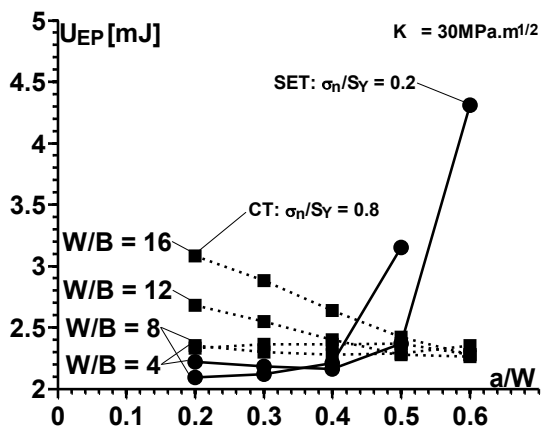


Figure 7. EP work inside the total pz volumes for several simulated cases.

3 EXPERIMENTAL PROCEDURE

The relatively new ASTM E1820 standard specifies procedures to measure EP toughness parameters J_{IC} , K_{JIC} , J_U , J_C , δ_{IC} , δ_U , and δ_C , in addition to J_R and δ_R curves measured in SEB, CT, and Disk-Shaped Compact Tension (DCT) specimens.

One of the available procedures for the measurement of fracture toughness is the so-called basic procedure, which requires multiple specimens to evaluate a single parameter. Another procedure is the elastic compliance technique, which generates J-R curves from several unloading/reloading sequences during the fracturing process to assess the fracture toughness parameters. This compliance procedure is used in this work, because it requires only a single specimen on the experiment, resulting in an economy of material.

3.1 Tensile tests

The specimens used in the present article are cut from an API 5L X80 steel plate with 21.85 mm thickness. Its tensile properties are measured by ASTM E8/E8M standard procedures, using three sub-sized plate specimens cut along the thickness in both transversal and longitudinal directions of the late. The average properties resulting from such tensile tests are listed in Table 2.

Table 2. Tensile average properties of the studied API 5L X80 steel.

Orientation	E [GPa]	S_Y [MPa]	S_U [MPa]	H [MPa]	h [1]
Transversal	231	546	627	954	0.139
Longitudinal	223	527	612	946	0.148

3.2 Toughness tests

For the toughness measurements, two 205 mm long, $W = 44.3$ mm, $B = 20.9$ mm SEB specimens are waterjet cut in a way that the crack would propagate on the transversal direction of the plate. An ultra-narrow notch with 20 mm depth from the surface is machined on a wire-cut electric discharge machine (EDM). All the specimen's dimensions are selected according to the ASTM E1820 standard.

3.2.1 Pre-cracked and side grooves

The ASTM E1820 requires that all fracture toughness specimens must be pre-cracked in fatigue. The crack length/specimen width ratio (a/W) chosen for the tests is in the middle of the range allowed by the standard ($a/W = 0.55$), so the target pre-crack size is 4.4 mm. During the fatigue cracking procedure, both specimens are subjected to three-point bending under force control, with $P_{max} = 0.9$ of the maximum allowed force and $R = P_{max}/P_{min} = 0.1$ under a frequency of 25 Hz. After 83,523 cycles, the SEB-1 developed a surface crack size of 4.04 mm, while the SEB-2 resulted in a 4.20 mm crack after 92,452 cycles. The crack sizes are measured using a microscope.

After fatigue pre-cracking, V-shaped side grooves with 10% of thickness (Figure 1) are applied on both surfaces of the specimens. The standard highly recommends this operation because it avoids crack tunneling and shear lips, besides ensuring a plane strain state and a straight crack front during the test. Therefore, B_N and the V-notch root radius (ρ) of the specimen are 16.72 mm and 0.5 mm, respectively.

3.2.2 J-R Curve and displacement fields

By the compliance procedures, during the loading of the specimen its crack opening displacement (COD) and/or its load-line displacement (LLD) must be continuously measured to obtain the J-R curve. In this work, the compliance test is controlled by the LLD with a speed of 0.003 mm/min. The first unloading/reloading point is chosen at a force range $0.75 \cdot P_{max}$, and the measurements include three unloading/reloading sequences. The consecutive unloading/reloading points have an interval of 0.1 mm in the COD, and sequences of three unloading/reloading are applied on the first 10 points. The force range in each point is $0.25 \cdot P_{max}$, so it could provide enough data points after the material relaxation. It is worth noting that the specimen suffered a

relaxation of almost 1 kN in every point after the plastic deformation. Thus, waiting 30 seconds for the relaxation in each point is necessary.

It is possible to measure the compliance in each unloading/reloading point, with the intention to estimate the crack size. The standard provides procedures for each specimen to incrementally calculate J for each measured compliance taking into account the elastic and plastic energies. The J-R curve is given by the assessed J and the crack extension (Δa) between the compliance points. Using the least squares method, it is possible to develop a linear regression of all J and Δa points, resulting in the J-R curve.

The displacement fields on the specimen surface are also simultaneously measured using the Correlated Solutions Volumetric DIC (VIC-3D) system (8). The device includes two 5-MP Point Grey GRAS-50S5M CCD digital cameras with a Tamron SP AF180mm F/3.5 lens attached to each camera, a regulable fiber-optic light source, standard calibration grids and a data acquisition system. The cameras are mounted on an adjustable tripod in front of the specimen. The complete experimental setup is shown in Figure 8.



Figure 8. Experimental setup used to measure the J-R curves and displacement fields on the specimen surface using the VIC-3D system.

It is not possible to apply here the standard procedure to determine the fracture toughness on the API 5L X80 steel, since the J-R curve grows higher than the J_{limit} defined by the standard. So, J_{IC} is evaluated from the intersection of the J-R curve with a 0.2 mm offset line, as illustrated in Figure 9. The measured fracture toughness is close from one specimen to another, 1145 kJ/m² for SEB-1 and 1111kJ/m² for SEB-2.

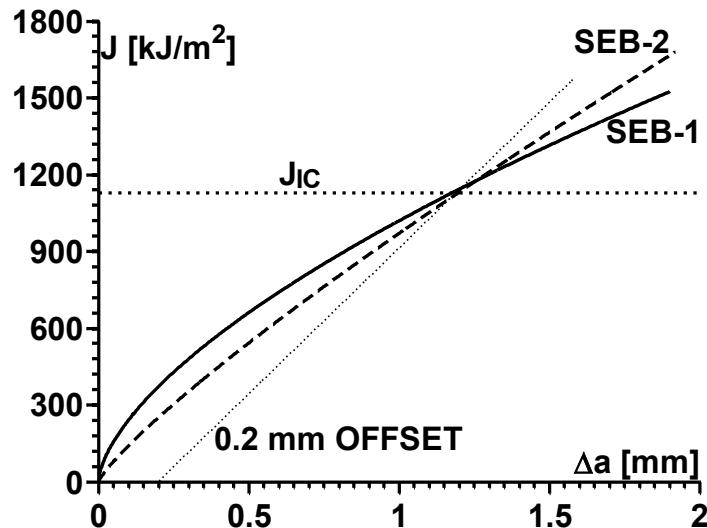


Figure 9. Measured J-R curves.

4 NUMERICAL VALIDATION

The experimental PL work (U_{PL}) up to the J_{IC} measured toughness value is compared with the U_{PL} results obtained directly from the volume of the pz calculated by the 3D EP FE model. The experimental U_{PL} is defined by the ASTM E1820 as the area (A_{pl}) under the force versus displacement record curve (Equation 5).

$$A_{pl(i)} = A_{pl(i-1)} + [P(i) + P(i-1)] [v_{pl(i)} - v_{pl(i-1)}] \cdot 0.5 \quad (5)$$

where P is the force, v_{pl} is the plastic part of the load line displacement (LLD) and ($A_{pl(i)} - A_{pl(i-1)}$) is the increment of the plastic area under the chosen P vs. LLD curve between lines of constant plastic displacement at points $(i-1)$ and (i) .

Figure 10 shows the experimental U_{PL} (ASTM E1820) in each compliance point varying with the LLD, indicating the critical PL work (U_{PL-C}) required to initiate the crack in the tested SEB specimen.

The numerical U_{PL} calculation is performed using Equation (6), which represents the summation of the U_{PL} work over all Gauss integration points inside the pz :

$$U_{PL} = V_e / 8 \times \sum_i^{8n} u_{pl} \quad (6)$$

where n is the number of elements inside the pz , V_e is the element volume and u_{pl} is the plastic work density in each Gauss integration point.

The difference between FE and ASTM E1820 U_{PL} results may be due to the effect of crack front tunneling on the fatigue pre-crack. The numerical model with straight crack fronts results in non-conservative U_{pl} calculations.

For all simulations, the LLD reference node is at the center of the roller. This node results in conservative U_{pl} predictions. By definition, the numerical LLD reference point is located in the middle of the uncracked ligament length, $0.5 \cdot (W + a)$.

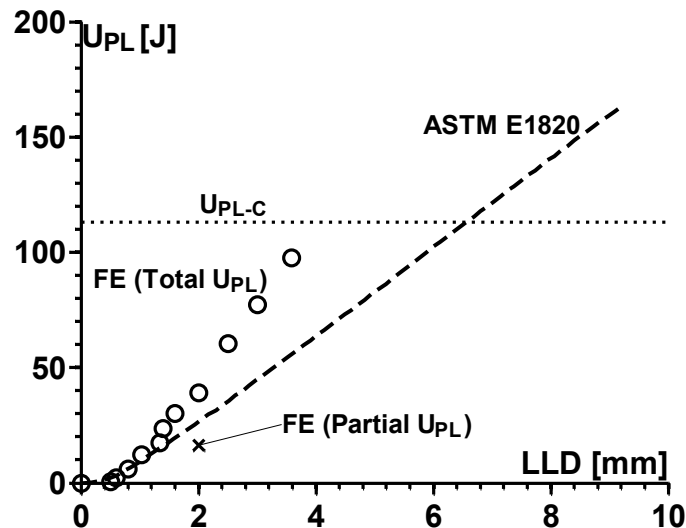


Figure 10. Numerical (FE) and experimental (ASTM E1820) incremental PL works (U_{PL}).

To calculate the PL work inside the pz , the $V_e/8$ criterion considers equal volume fractions for each integration points per FE. On the other hand, the SEB specimen model is meshed with some distorted elements due to its side grooves. Therefore, errors in U_{pl} calculations might be generated using this criterion. To solve this problem, the exact volume fractions should be calculated. This new criterion will be implemented to be applied in future analyses.

The numerical U_{pl} is the sum of the PL work inside the pz developed around the crack front and the PL work due to the contact surfaces between the cylinder roller and the SEB specimen. This total U_{PL} may also result in conservative predictions. Thus, it is worth evaluating each PL work, as presented in detail for $LLD = 2$ mm in Figure 10. For this displacement, there are two numerical analyses for U_{PL} . The first one is the total U_{PL} , clearly giving the highest and conservative PL work. The second is calculated through the partial pz volume up to the middle of the uncracked ligament length, resulting in a conservative prediction. A third analysis should be performed from the effective plastic energy inside the pz around the crack front, calculated from the difference between the total U_{PL} and the PL work due to the contact surfaces between the cylinder roller and the SEB specimen without a crack. Finally, the measured horizontal and transversal x-y plane displacements are compared with the results obtained from the 3D EP FE sub-model for an applied displacement, $LLD = 8.55$ mm.

As it can be seen in Figures 11 and 12, the agreement between numerical (FE) and experimental (DIC) displacement results is good. For the horizontal displacements shown in Figure 11, there is a change in slope near the crack tip region in both FE and DIC data. This gap is caused by the tunneling effect that often occurs during fatigue pre-cracks, as noted elsewhere (3). Thus, these discrepancies probably can be alleviated modeling the actual curvature along the crack front. For transversal displacements (Figure 12), the magnitude is reduced from approximately -0.36 mm at the side groove edge to an almost null value at 9.15 mm from the crack plane slightly ahead of the crack tip. The difference between FE and DIC results may be due to the same tunneling effect. It is also difficult to determine a reference point due to the impossibility of measuring displacements at free edges. Nevertheless, note that there are relatively few differences between the FE and DIC results.

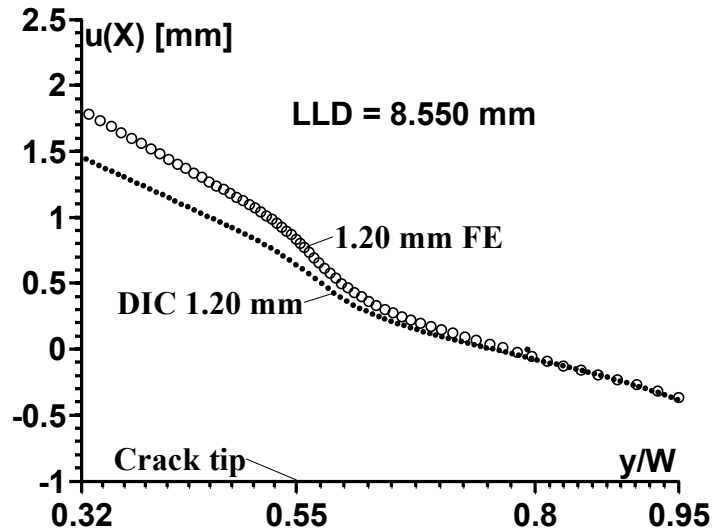


Figure 11. Numerical (FE) and experimental (DIC) horizontal displacement ($u(X)$) fields at 1.2 mm from the crack plane for an applied displacement $LLD = 8.55$ mm.

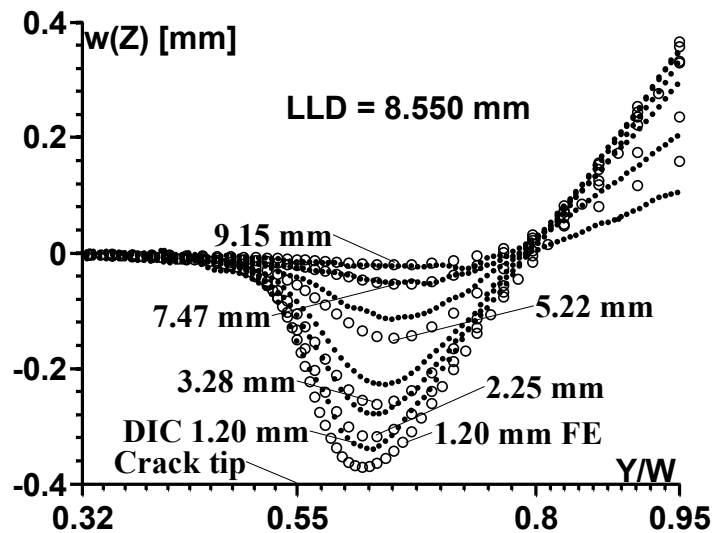


Figure 12. Numerical (FE) and experimental (DIC) displacement ($w(Z)$) fields in the transversal x-y plane at different distances (1.2 - side groove edge, 2.25, 3.28, 5.22, 7.47 and 9.15 mm) from the crack plane for an applied displacement $LLD = 8.55$ mm.

5 CONCLUSIONS

This work presented 3D p_z estimates using a 3D EP sub-modeling FE technique. The results obtained using this technique are validated through numerical and experimental results found in the literature. In addition, the methodology for the calculation of p_z volumes considering the $V_e/8$ improved criterion was verified from numerical simulations, where a minimum of 15 elements per modeled thickness $B/2$ are needed to reach convergence. Finally, the results obtained using the 3D EP FE model are validated through direct comparison with experimental results for the PL work up to the J_{IC} measured toughness values as well as displacements measured on the surface of the specimen using 3D DIC techniques. The comparisons between numerical and experimental results indicate good correlations.

Acknowledgements

The authors would like to thank the Brazilian funding agency CAPES for the scholarships granted, and USIMINAS for supplying the material used in the tests.

REFERENCES

- 1 ASTM E1820–17, “Standard Test Method for Measurement of Fracture Toughness”, American Society for Testing and Materials, 2017.
- 2 Cravero S, Ruggieri C. Estimation procedure of Jresistance curves for SE(T) fracture specimens using unloading compliance. Eng Fract Mech, 74 (2007) 2735–2757.
- 3 Michael Besel , Eric Breitbarth. Advanced analysis of crack tip plastic zone under cyclic loading. International Journal of Fatigue, 93 (2016) 92–108.
- 4 Camas D et al. Numerical and experimental study of the plastic zone in cracked specimens. Engineering Fracture Mechanics, 185 (2017) 20-32.
- 5 K. Wallin. The size effect in K_{IC} results. Eng. Fract. Mech., 22 (1985), pp. 149-163.
- 6 T. L. Anderson, Fracture Mechanics: Fundamentals and Applications, third ed., Taylor & Francis, (2005).
- 7 ANSYS 13.1 help//Mechanical APDL (formerly ANSYS)//Advanced analysis techniques guide//9. Sub modeling.
- 8 VIC-3D 2010, Correlated Solution Inc., <http://www.correlatedsolutions.com/>.